Environmental Research 171 (2019) 395–402

Contents lists available at ScienceDirect

Environmental Research

journal homepage: www.elsevier.com/locate/envres

Development of an advanced electrochemical biosensing platform for *E. coli* using hybrid metal-organic framework/polyaniline composite

Arushi Gupta[a,b], Sanjeev K. Bhardwaj[a,b], Amit L. Sharma[a,b], Ki-Hyun Kim[c,*], Akash Deep[a,b,**]

[a] CSIR-Central Scientific Instruments Organisation (CSIR-CSIO), Sector 30C, Chandigarh 160030, India
[b] Academy of Scientific and Innovative Research, CSIO-AcSIR, Sector 30C, Chandigarh 160030, India
[c] Department of Civil and Environmental Engineering, Hanyang University, 222 Wangsimni-Ro, Seoul 04763, Republic of Korea

ARTICLE INFO

Keywords:
Metal-organic framework
Conducting polymer
Biosensor
Bacteria
E. coli
Environmental sample

ABSTRACT

Because of numerous merits (e.g., the possibility of their synthesis in 1-D, 2-D, and 3-D forms, large surface-to-volume ratio, and flexible framework functionality), metal-organic frameworks (MOFs) are envisaged as excellent media for the development of biosensors for diverse analytes present in environmental media. The present research work, for the first time, reports the development of a Cu-MOF based electrochemical biosensor for highly sensitive detection of *E. coli* bacteria. In order to realize an MOF-based electrochemically active platform, $Cu_3(BTC)_2$ (BTC = 1,3,5-benzenetricarboxylic acid) was mixed with polyaniline (PANI). The spectroscopic/morphological characterizations of the resulting composite were established with the aid of FT-IR, UV–visible spectroscopy, X-ray diffraction, electron microscopy, and surface area analysis. The thin films of $Cu_3(BTC)_2$-PANI, on an indium-tin oxide (ITO) substrate, were bio-interfaced with anti-*E. coli* antibodies for use as a novel biosensing electrode. Based on the electrochemical impedance spectroscopy (EIS) technique of signal measurement, the above sensor exhibited high sensitivity to detect very low concentrations of *E. coli* (2cfu/mL) in a short response time (~2 min) and was also selective in the presence of other non-specific bacteria. As a novel highlight of the research, this new MOF/PANI based detection platform for *E. coli* has shown improved performance than many of the previously reported electrochemical biosensors.

1. Introduction

Among the various types of techniques available for the analysis of biomolecules, the electrochemical biosensors have acquired a special recognition due to a number of beneficial features such as portability, on-site detection capability, low-cost, rapid detection time, sensitivity, and selectivity (Hernandez-Vargas et al., 2018; Liu et al., 2018; Zhu et al., 2014). The transducer surface and biorecognition probes generally represent the two major components of an electrochemical biosensor. The advent of nanomaterials has replaced conventional transducers by providing better charge conduction characteristics and enhanced surface areas for a better binding of biorecognition probes. In recent years, a list of nanomaterials (like graphene, carbon nanotubes (CNTs), quantum dots (QDs), nanopolymers, and molybdenum disulphide nanosheets) have been proposed and demonstrated as the materials of choice in the construction of highly sensitive electrochemical biosensors (Maduraiveeran and Jin, 2017; Kokkinos et al., 2015). The main biorecognition molecules used in the electrochemical biosensors may be listed as antibodies, enzymes, peptides, aptamers, whole cells, and nucleic acids (Lei et al., 2014; Kumar et al., 2015; Zhao et al., 2014; Zhu et al., 2013). The antibody-based biosensors have flourished due to their high affinity toward the target analytes.

E. coli is one of the most prevalent pathogens causing several food and water borne diseases (Muniesa et al., 2018; Thakur et al., 2018; Wildeboer et al., 2010). Its detection with electrochemical biosensors has been reported by exploiting nanosurfaces such as graphene (Justino et al., 2017), graphene-gold or graphene-silver nanoparticle composites (Wang et al., 2014), standing paper electrode (Wang et al., 2013), gold nanoparticles-superparamagnetic microbeads (Hassan et al., 2015), indium-tin oxide layers (dos Santos et al., 2015), and polymeric nanoparticles (Xu et al., 2016).

Metal-organic frameworks (MOFs) have attracted great research interest in recent years. They have been explored for a wide range of applications, e.g., in drug delivery, gas storage, catalysis, molecular sensing, photovoltaics, supercapacitors, and optics (Della Rocca et al., 2011; Kent et al., 2011; Li et al., 2014; Si et al., 2011; Zhang et al.,

* Corresponding author.
** Corresponding author at: CSIR-Central Scientific Instruments Organisation (CSIR-CSIO), Sector 30C, Chandigarh 160030, India.
E-mail addresses: kkim61@hanyang.ac.kr (K.-H. Kim), dr.akashdeep@csio.res.in (A. Deep).

https://doi.org/10.1016/j.envres.2019.01.049
Received 6 November 2018; Received in revised form 7 January 2019; Accepted 29 January 2019
Available online 30 January 2019
0013-9351/

2014). In context to their applications as sensory material, MOFs possess an ordered structure with strong chemical bonds that make them environmentally stable (Allendorf and Stavila, 2015). MOFs are also known as highly porous and large surface area crystalline materials that can be customized as per the specifications of targeting structures (Ahmed and Jhung, 2014; Bhardwaj et al., 2016b). Such modifications can be done through certain strategies, such as selection of appropriate metal centres and functional linkers, doping of molecules and nanoparticles, and formation of MOF-composites with other functional materials (Schoedel et al., 2016).

The application of MOFs as transducer surface in electrochemical biosensors has been proposed in some recent works; e.g. for the detection of prostate specific antigen (Bhardwaj et al., 2017) and pesticides (Bhardwaj et al., 2015). A line of evidence indicates that the MOFs can be employed as efficient transducer surfaces for the development of antibody based electrochemical biosensors. Owing to their hierarchical synthesis, the application of MOFs offers an important advantage of material reproducibility which cannot easily be recognized by other nanomaterial surfaces like graphene, CNTs, and MoS_2. Moreover, the MOF based surfaces can also be projected as more biocompatible and easily disposable without concerns of nanotoxicity (Li et al., 2012).

In the present research work, for the first time, we propose the application of a MOF/antibody interface for the assembly of an electrochemical immunosensor for *E. coli*. To this end, $Cu_3(BTC)_2$ (or also known as HKUST-1 or MOF-199) has been chosen in view of its facile synthesis and features like large surface area, high pore volume, and high thermal stability. Previously, $Cu_3(BTC)_2$ has been reported for diverse applications, such as gas storage, catalysis, and sensing of analytes (like methanol, ethanol, propanol, and nitric oxide) (Ameloot et al., 2009; Campbell and Dincă, 2017; Davydovskaya et al., 2014; Guo et al., 2009; Hosseini et al., 2016; Maes et al., 2010). Because of a non-conducting nature of $Cu_3(BTC)_2$, it is required to introduce or mix some additional electroactive species so as to realize a $Cu_3(BTC)_2$ based electrochemical platform. In this context, we have chosen polyaniline (PANI) of which addition has resulted in the introduction of electrical conductivity in a $Cu_3(BTC)_2$/PANI composite structure while also helping the formation of a homogenous thin film of the composite material over the electrode surface. This thin film electrode was subsequently interfaced with the anti- *E. coli* antibodies (Ab). The electrochemical impedance spectroscopy based operation of the Ab/$Cu_3(BTC)_2$/PANI sensor has offered highly sensitive detection of *E. coli*. The biosensor has also been demonstrated to be highly efficient for the determination of *E. coli* in some spiked real samples. The enhanced performance of the herein proposed MOF based electrochemical sensor over most of the previously reported electrochemical sensors for *E. coli* should be attributed to factors such as large surface area of the transducer surface (to support improved antibody loading) and ready-availability of functional groups (for robust bioimmobilization).

2. Experiment

2.1. Materials and equipment

All the reagents and solvents used in this study were of analytical grade purity and purchased from Sigma (India) or Merck (India). The experiments were carried out at room temperature conditions (RT, 25 ± 2 °C). UV–Vis (Varian Cary 5000) and Fourier transform infrared (FTIR, Perkin Elmer, Spectrum Two) spectrophotometers were used for the basic characterization of the samples. The structural, morphological, and topological studies were carried out using field emission-scanning electron microscope (FE-SEM, Hitachi, S4300 SE/N) and X-ray diffractometer (Brooker D8 Advanced, Kα = 1.54 Å). Nitrogen isotherm analysis was performed using a BELSORP-max sorptometer (Microtrac). Before analysing the surface area, the samples were degassed at 120 °C for 20 h. The current-voltage (I-V) parameters were studied on a semiconductor characterization system (Keithley, Model 4200).

2.2. Synthesis of $Cu_3(BTC)_2$

$Cu_3(BTC)_2$ was prepared by following a previously published protocol (Israr et al., 2016). Briefly, 2.38 mM of benzene-1,3,5-tricarboxylic acid (H_3BTC) (98%) was mixed (by stirring) with 4.34 mM of $Cu(NO_3)_2{\cdot}3H_2O$ in 100 mL solvent mixture of deionized water, ethanol, and DMF (1:1:1, v/v). Subsequently, 0.5 mL of triethylamine (TEA) was added, and the resulting mixture was ultrasonicated (bath sonication) at RT for 45 min. It led to the precipitation of blue coloured crystals, which were then separated through centrifugation (12,000 rpm, 10 min). The product was washed with water and ethanol before drying overnight at 70 °C under vacuum.

2.3. Synthesis of $Cu_3(BTC)_2$-Polyaniline composite films and immobilization of antibody

The formation of the $Cu_3(BTC)_2$-Polyaniline composite ($Cu_3(BTC)_2$-PANI) was achieved by first mixing 100 mg of PANI (emeraldine salt, Sigma-Aldrich, average Mw ~ 15,000, dark green powder) with linker (H_3BTC) and then initiating the formation of the MOF as aforementioned. The formed product $Cu_3(BTC)_2$-PANI was purified by washing with water and ethanol before drying overnight at 70 °C under vacuum.

Thin films of $Cu_3(BTC)_2$-PANI were prepared on ITO (indium tin oxide) slides by drop casting technique (schematic shown in Fig. 1). A viscous slurry of the coating material in presence of n-methyl pyrrolidine (NMP) solvent was used during the electrode formation process. The electrodes were washed with ethanol and left to anneal at 100 °C for ensuring the robustness of the coatings. The prepared several sets of $Cu_3(BTC)_2$-PANI electrodes were further incubated with a 2.38 mM of H_3BTC suspension (in 1:1:1 v/v solvent mixture of water, ethanol, and DMF; time = 30 min) in order to obtain the terminal -COOH groups. The modified electrodes were then incubated with a mixture of 0.05 M EDC [(1-ethyl-3-(3-(dimethylamino)propyl) carbodiimide] and 0.01 M NHS (N-hydroxysuccinimide) in PBS for 2 h. Next, the EDC-NHS activated $Cu_3(BTC)_2$-PANI/ITO electrodes were allowed to incubate with 10 μL (1 μg/mL) of antibody solution (in PBS buffer, pH 7.4) for 1 h. The prepared bioelectrodes were then washed with 0.01% Tween-20 in order to block the non-specific binding sites (Buchwalow et al., 2011). The finally prepared bioelectrodes (Ab/ $Cu_3(BTC)_2$-PANI/ITO) were again washed with PBS buffer before storing them under refrigerated

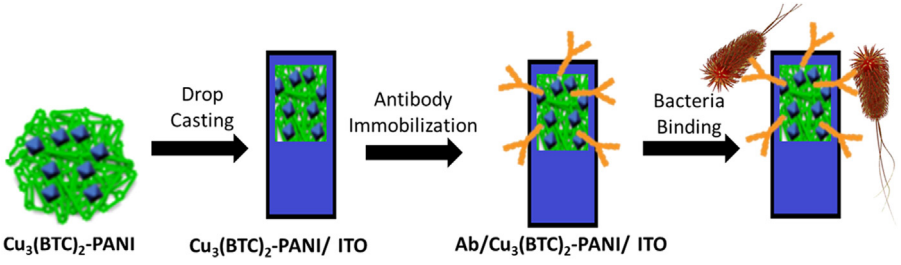

Fig. 1. Schematic of procedure for bioelectrode fabrication and its subsequent utilisation for impedimetric sensing of *E. coli*.

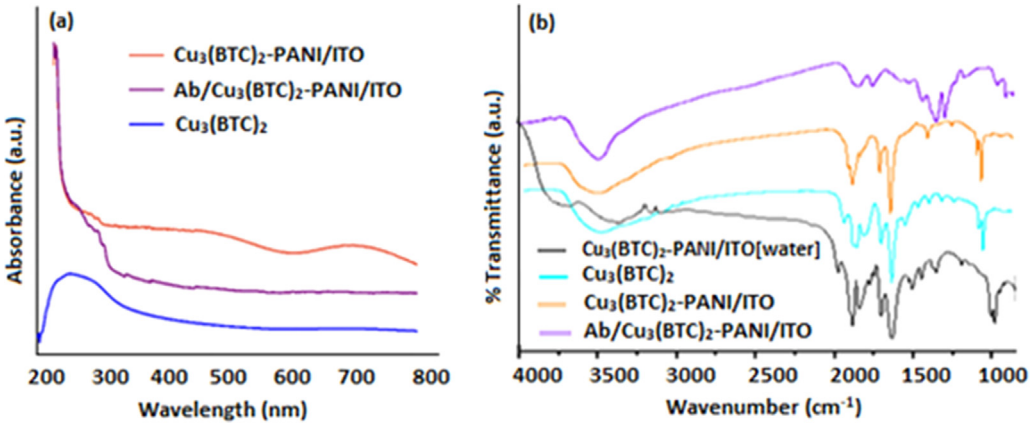

Fig. 2. (a) UV–Vis spectra of PANI-$Cu_3(BTC)_2$/ITO and Ab/PANI-$Cu_3(BTC)_2$/ITO; (b) FTIR spectra of $Cu_3(BTC)_2$, $Cu_3(BTC)_2$-PANI/ITO, $Cu_3(BTC)_2$-PANI/ITO$_{[water]}$, and Ab/$Cu_3(BTC)_2$-PANI/ITO.

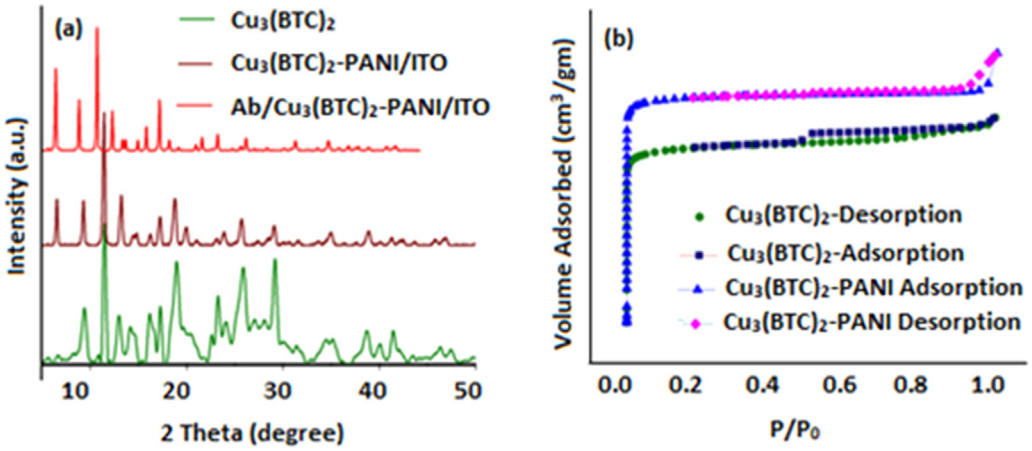

Fig. 3. (a) XRD spectra of $Cu_3(BTC)_2$, $Cu_3(BTC)_2$-PANI /ITO and Ab/$Cu_3(BTC)_2$-PANI/ITO; (b) N_2 adsorption-desorption isotherms of $Cu_3(BTC)_2$ and $Cu_3(BTC)_2$-PANI samples.

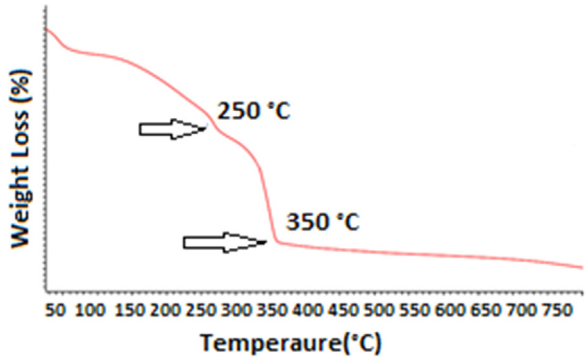

Fig. 4. Thermo gravimetric analysis of $Cu_3(BTC)_2$-PANI.

conditions (4 °C).

2.4. Application of Ab/$Cu_3(BTC)_2$-PANI/ITO biosensor for impedimetric detection of E. coli

Electrochemical impedance spectroscopy (EIS) technique was used to evaluate the performance of Ab/$Cu_3(BTC)_2$-PANI/ITO bioelectrodes for electrochemical detection of *E. coli*. A stock solution of 2×10^8 cfu/mL *E. coli* was prepared after standardizing the bacteria concentration with standard colony counting method. This stock bacteria solution was diluted to prepare other known concentrations (e.g., 10^2X, 10^3X, and 10^4X). During the analysis step, 10 µL aliquot of each of the known concentrations of *E. coli* was exposed to the Ab/$Cu_3(BTC)_2$-PANI/ITO bioelectrodes for 10 min. After the formation of antibody-antigen complex, the EIS characteristics of the bioelectrode were investigated in a standard ferro-ferri electrolyte solution (5 mM $K_3Fe(CN)_6$ + 5 mM $K_4Fe(CN)_6 \cdot 3H_2O$ in 0.1 M PBS). During the EIS studies, AC frequencies were varied within a range of 0.1 Hz-1 MHz at an amplitude of 5 mV.

3. Results and discussion

3.1. Spectroscopic characterization of $Cu_3(BTC)_2$, $Cu_3(BTC)_2$-PANI/ITO, and Ab/$Cu_3(BTC)_2$-PANI/ITO

The completion of bio-interfacing of the anti- *E. coli* antibodies over the $Cu_3(BTC)_2$-PANI/ITO substrate was checked through UV–Vis and FTIR based characterizations. Fig. 2a provides the energy absorption profiles of $Cu_3(BTC)_2$, $Cu_3(BTC)_2$-PANI/ITO, and Ab/$Cu_3(BTC)_2$-PANI/ITO samples. The first sample showed a broad peak around 260 nm due to ligand-to-metal charge transfer (LMCT) transitions from oxygen to copper ions (Cu^{2+}) (Bhardwaj et al., 2017). In case of the analysis of $Cu_3(BTC)_2$-PANI/ITO sample, the LMCT reporting peak was slightly shifted to 360 nm (from the original value of 300 nm). This can be attributed to the change in hydration conditions and coordination spheres of copper ions. More specifically, the red shift may represent the removal of water molecules from the MOF cages. This condition increased the electron density on carboxylate groups (or ionicity of Cu(II) ions) (Prestipino et al., 2006; Schlichte et al., 2004). In the sample of Ab/$Cu_3(BTC)_2$-PANI/ITO, the appearance of a new protein specific peak at

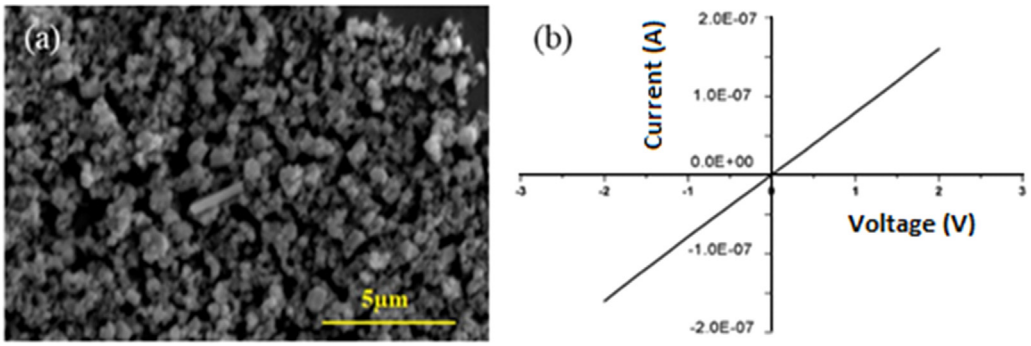

Fig. 5. (a) FE-SEM of $Cu_3(BTC)_2$-PANI composite deposited on ITO surface; (b) Current-Voltage property of $Cu_3(BTC)_2$ -PANI/ITO surface.

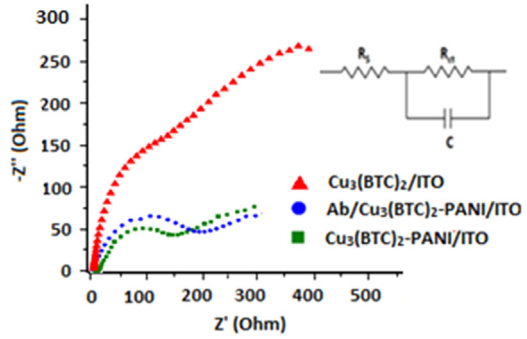

Fig. 6. Nyquist plots of ITO, $Cu_3(BTC)_2$-PANI, $Cu_3(BTC)_2$ -PANI and Ab/$Cu_3(BTC)_2$-PANI.

280 nm confirmed successful biointerfacing of the antibodies with $Cu_3(BTC)_2$-PANI/ITO (Wu et al., 2016).

Fig. 2b shows the FTIR analysis results for several samples, including $Cu_3(BTC)_2$, $Cu_3(BTC)_2$-PANI/ITO, $Cu_3(BTC)_2$-PANI/$ITO_{[water]}$ (i.e., $Cu_3(BTC)_2$-PANI/ITO electrode contacted with PBS for 2 h), and Ab/$Cu_3(BTC)_2$-PANI/ITO. The bands around 1618 and 1560 cm^{-1} were associated with the ligand component (i.e., BTC) of the MOF (Yan et al., 2014; Zeng et al., 2013). Specifically, these bands corresponded to the asymmetric stretching of carboxylate groups. Further, the bands around 1444 and 1374 cm^{-1} were attributable to the symmetric stretching of carboxylate group (Deep et al., 2012). The metal ion (Cu center) and linker (C-H band) specific bands at around 492 and 757 cm^{-1}, respectively also verified the integrity of MOF in the Ab/$Cu_3(BTC)_2$-PANI/ITO sample (Daoben et al., 1982). The bands between 2500 and 3500 cm^{-1} represented the bending and stretching frequencies of O-H groups from the incorporated solvent or water molecules (Peng et al., 2014). In case of the PANI containing samples, an additional peak at 806 cm^{-1} appeared due to the plane bending of the benzene ring (Trchová and Stejskal, 2011).

It should be noted that the FTIR analysis of $Cu_3(BTC)_2$-PANI/$ITO_{[water]}$ also contained all the characteristic peaks observed in the $Cu_3(BTC)_2$-PANI/ITO sample. This observation was important to conclude that the $Cu_3(BTC)_2$-PANI/ITO electrode was structurally stable (i.e., intact functionality) even after being in extended contact (e.g., at least up to 2 h) with an aqueous solution. Hence, there was no apparent risk of sensor destabilization in subsequent processing steps, e.g., the interfacing of biomolecules over the electrode and the application of the resulting bioelectrode in actual sensing experiment.

FTIR analysis also verified the presence of antibodies in the Ab/$Cu_3(BTC)_2$-PANI/ITO electrode through the appearance of an additional band at 1640 cm^{-1}, attributing to the N = C vibrations (a characteristic of the protein amide bonds). Thus, the above discussed UV–Vis and FTIR results clearly highlight a successful formation of the Ab/$Cu_3(BTC)_2$-PANI/ ITO bioelectrode.

3.2. Structural and morphological characterizations

The powder XRD patterns of $Cu_3(BTC)_2$ and $Cu_3(BTC)_2$-PANI/ITO samples are shown in Fig. 3a. The XRD pattern of $Cu_3(BTC)_2$ contained standard peaks as reported in literature (Chui et al., 1999; Mustafa et al., 2011). For $Cu_3(BTC)_2$-PANI/ITO, the peaks between 10° and 30° were due to the parallel and perpendicular periodicity of PANI. Further, the XRD pattern of Ab/$Cu_3(BTC)_2$-PANI/ITO sample has been found encompassing all the typical peaks of both $Cu_3(BTC)_2$ and PANI. The above study confirmed that the adsorption of antibodies over the $Cu_3(BTC)_2$-PANI/ITO surface has not affected the crystallinity of the composite material.

Fig. 3b shows the N_2 adsorption and desorption plots for the $Cu_3(BTC)_2$ and $Cu_3(BTC)_2$-PANI samples. The observed isotherms for both the samples were typical for the mesoporous materials (Peng et al., 2014). Langmuir surface area of $Cu_3(BTC)_2$ was estimated to be 1091 m^2/g with a pore volume of 0.53 cm^3g^{-1}. Its value was however reduced to 868 m^2/g after the incorporation of PANI. This reduction in the overall surface area value reflected the successful introduction of

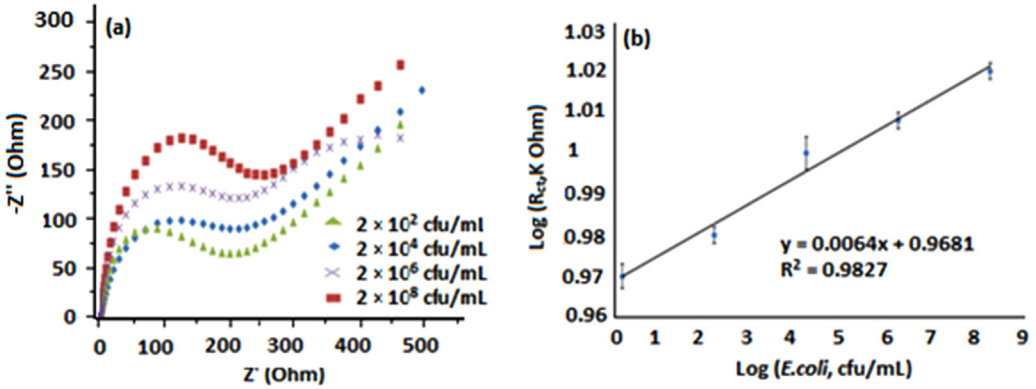

Fig. 7. The basic QA information of fabricated biosensor (Ab/$Cu_3(BTC)_2$-PANI/ITO): (a) Nyquist plots of the fabricated biosensor (Ab/$Cu_3(BTC)_2$-PANI/ITO) upon exposures to different concentration of *E. coli*; and (b) Calibration curve for the developed Ab/$Cu_3(BTC)_2$-PANI/ITO biosensor (Variation in the values of charge transfer resistance with respect to the number of bacterial colonies analyzed (2, 2 × 10^2, 2 × 10^4, 2 × 10^6 and 2 × 10^8 cfu/mL *E. coli*).

Table 1
Performance comparison between various electrochemical nanosensors employed for the detection of *E. coli*.

Order	Nanomaterial	Technique	Linear Detection range (cfu/mL)	Limit of detection (cfu/mL)	Refs.
1.	Alumina nanoporous membrane/ hyaluronic acid	Electrochemical impedance spectroscopy	$10–10^5$	83	(Joung et al., 2013)
2.	Gold electrodes via a self-assembled monolayer (SAM) of mercaptohexadecanoic acid	Electrochemical impedance spectroscopy	3×10^{-3} - 10^4	2	(Dos Santos et al., 2013)
3.	Gold nanoparticles modified free-standing graphene paper electrode	Electrochemical impedance spectroscopy	1.5×10^2 - 1.5×10^7	–	(Wang et al., 2013)
4.	Polymeric nanocomposites (PMNCs) modified screen-printed interdigitated microelectrodes (SP-IDMEs)	Electrochemical impedance spectroscopy	–	10^2	(Xu et al., 2016)
5.	Multiwall carbon nanotube-polyallylamine modified screen- printed electrode (MWCNT-PAH/SPE	Amperometric	$1 \times 10^3 – 5 \times 10^5$	800	(Viswanathan et al., 2012)
6.	Single walled carbon nanotubes	Potentiometric	10^4	6	(Zelada-Guillén et al., 2010)
7.	Graphene	Conductometric	–	10	(Huang et al., 2011)
8.	**Ab/$Cu_3(BTC)_2$-PANI/ITO**	**Electrochemical impedance spectroscopy**	**$2.0 – 2 \times 10^8$**	**2**	**Present work**

PANI within the $Cu_3(BTC)_2$ matrix.

The thermal stability of the $Cu_3(BTC)_2$-PANI composite material has been investigated by thermal gravimetric analysis. The results seen in Fig. 4 indicated an initial weight reduction due to the loss of absorbed water/solvent molecules. After that, there was an insignificant weight loss until 250 °C to highlight an excellent thermal stability of the $Cu_3(BTC)_2$-PANI composite. The degradation of the sample took place at 350 °C (and beyond) as a result of breaking down of linker molecules.

The FE-SEM imaging of the $Cu_3(BTC)_2$-PANI/ITO sample is presented in Fig. 5a. This investigation clearly indicated the crystalline nature of the material. The synthesized material was of a homogenous nature with lateral crystallite dimensions in range of 100–200 nm.

3.3. Performance of the synthesized Ab/$Cu_3(BTC)_2$-PANI/ITO sensor

The electrical conduction property of the $Cu_3(BTC)_2$-PANI substrate was assessed by its current-voltage (I-V) characteristics. The corresponding I-V plot is shown in Fig. 5b. It must be noted there that pure $Cu_3(BTC)_2$ film has a non-conducting surface. Its composite formation with PANI has resulted in the introduction of a useful level of electrical conductivity. As seen in Fig. 4b, the $Cu_3(BTC)_2$-PANI/ITO showed an ohmic conductivity profile with an average film resistance of 13.3 MΩ. The I-V characteristics were also investigated after the attachment of antibodies. The resulting Ab/$Cu_3(BTC)_2$-PANI/ITO sensor showed a base resistance value of 15 MΩ. An increase in the film resistance after the attachment of antibodies may be attributed to the less conducting nature of the Ab/$Cu_3(BTC)_2$-PANI/ITO surface after it was decorated with protein structure (i.e., antibodies).

EIS (electrochemical impedance spectroscopy) technique is a popular electrochemical technique for developing immunosensors. The sensor output is obtained in the form of Nyquist plot which is then used to compute R_{ct} (charge transfer resistance) values by applying suitable data fitting. A Nyquist plot (typically with a semicircle shape) incorporates data from different frequency points and the real and imaginary components are described on Y- and X- axis, respectively.

We have carried out the EIS investigations on our different electrodes using the standard ferro-ferri electrolyte media. Nyquist plots for the $Cu_3(BTC)_2$/ITO, $Cu_3(BTC)_2$-PANI/ITO, and Ab/$Cu_3(BTC)_2$-PANI/ITO platforms are provided in Fig. 6. The values of R_{ct} have been calculated by successfully fitting the curves in to Randell's circuit (inset of Fig. 6). These values for $Cu_3(BTC)_2$/ITO, $Cu_3(BTC)_2$-PANI/ITO, and Ab/$Cu_3(BTC)_2$-PANI/ITO were estimated as 206, 5.3, and 8.4 KΩ, respectively. The above values were on the expected lines, showing a good agreement with the behaviour of many other earlier reported EIS based immunosensors (Bhardwaj et al., 2016a).

The response of the Ab/$Cu_3(BTC)_2$-PANI/ITO sensor (Nyquist plots) toward different levels of bacterial concentration (2.0–2.0 × 10^8 cfu/mL *E. coli*) is summarized in Fig. 7a. The corresponding calibration curve is shown in Fig. 7b. Nyquist plots were characterized with increasing semicircle diameter with the increasing bacteria concentration. Such electrochemical behaviour from EIS based biosensors has been documented and explained in many previous studies (Dos Santos et al., 2013). It is clear that our biosensor was able to offer a linear response over a wide range of *E. coli* concentration, i.e, 2.0–2.0 × 10^8 cfu/mL. The limit of detection (LOD) of the proposed sensor has been calculated by the expression: LOD = 3σ (Bhardwaj et al., 2016a) and found to be 2 cfu. A comparison between the above obtained values of range of detection and LOD with those reported earlier with other electrochemical biosensors clearly suggests that the present Ab/$Cu_3(BTC)_2$-PANI/ITO sensor is an efficient platform in terms of all the critical QA parameters (Table 1).

The Ab/$Cu_3(BTC)_2$-PANI/ITO biosensor has also been investigated for various other important parameters like inter-/intra- assay precision, long-term storage stability, and specificity. The intra- and inter-assay precision measurements were used to carry out to establish the reproducibility of this biosensing system. For inter-assay analysis,

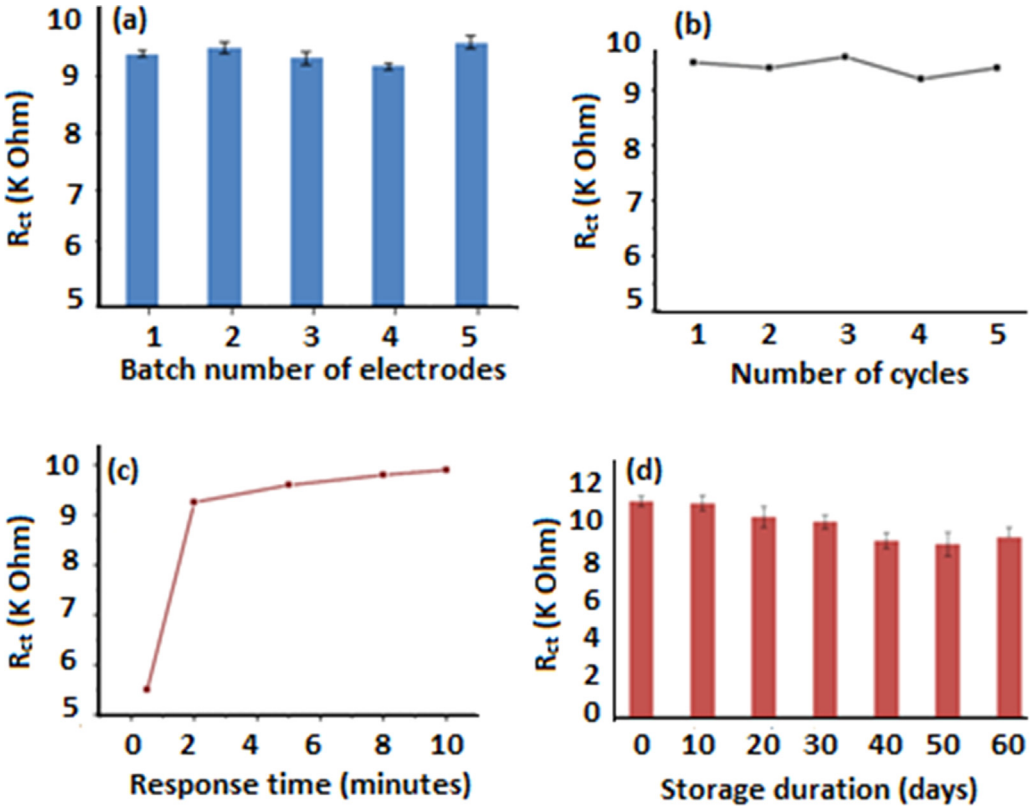

Fig. 8. (a) Responses of different batches of prepared Ab/$Cu_3(BTC)_2$-PANI sensors; (b) Response of Ab/$Cu_3(BTC)_2$-PANI sensor at fixed concentration over 5 successive cycles; (c) Response time of prepared bioelectrode towards *E. coli*; (d) Stability of the Ab/$Cu_3(BTC)_2$-PANI/ITO biosensor with respect to its long-duration storage. *Note: The concentration of E. coli taken in all the above studies was fixed to* 2×10^2 *cfu/mL.*

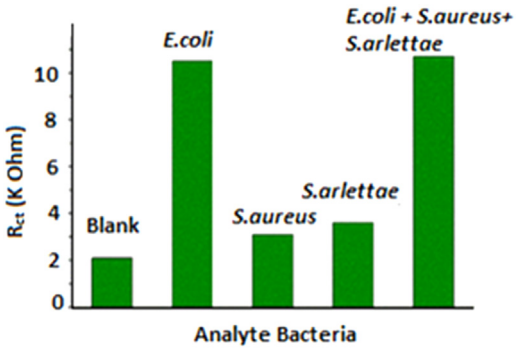

Fig. 9. Results on the specificity testing of Ab/$Cu_3(BTC)_2$-PANI biosensor toward *E. coli* in presence of other non-specific bacteria [*E. coli* = 2×10^2 cfu/mL; *S. aureus* and *S. arlettae* = 2×10^6 cfu/mL].

sensor response was checked against a fixed bacterial concentration with five independent sensor electrodes prepared under similar experimental conditions. The response was found to be highly compatible with each other (Fig. 8(a)). For intra-assay analysis, sensor response was checked against a fixed 2×10^2 cfu/mL concentration repetitively over five times. These studies also confirmed about the signal stability (Fig. 8(b)). Hence; the above studies gave suitable confirmation about the reproducibility of the sensor. The response time of the Ab/$Cu_3(BTC)_2$-PANI/ITO biosensor has also been studied. For this, the electrodes were incubated with a fixed concentration of bacteria for different time periods. The results of the study highlighted that 2 min were sufficient to achieve stable reading (Fig. 8(c)).

The specificity of the developed Ab/$Cu_3(BTC)_2$-PANI /ITO has also been investigated (Fig. 9). The sensor was found to be extremely specific without the alteration of effective impedance in the presence of potential interfering non-specific bacteria (*S. arlettae* and *S. aureus*). The long-term stability of the fabricated sensor was also recorded. For this study, the fabricated biosensors were stored under refrigerated conditions (4 °C). The sensor response was found to be significantly stable for up to at least 60 days of storage (Fig. 8(d)).

Finally, a test of the practical utility of the Ab/$Cu_3(BTC)_2$-PANI/ITO sensor was made by extending its application toward bacterial detection in spiked real water samples. The results of this test are presented in Table 2. The analyte concentration detected with the herein developed biosensor was in close agreement with the analytical data

Table 2
Analysis of *E. coli* in spiked samples of lake water along with the results of validation studies with colony counting method.

Spiked concentration of *E. coli*	Response of sensor and number of corresponding colonies detected	Data from colony counting technique
Unknown (cfu/mL)	R_{ct} - 14 KΩ Bacterial concentration in solution = 3.2×10^6 cfu/mL	3×10^6 cfu/mL
Unknown (10^2X dilution)	R_{ct} - 13.6 KΩ Bacterial concentration in solution = 3.2×10^5 cfu/mL	3×10^5 cfu/mL
Unknown (10^3X dilution)	R_{ct} - 12.4 KΩ Bacterial concentration in solution = 2.9×10^4 cfu/mL	3×10^4 cfu/mL
Unknown (10^4X dilution)	R_{ct} - 10.8 KΩ Bacterial concentration in solution = 3.06×10^2 cfu/mL	3×10^2 cfu/mL

Note: A stock solution of unknown bacterial concentration was synthetically prepared. Its serial dilutions were analyzed with the Ab/$Cu_3(BTC)_2$-PANI/ITO sensor. Validation of the results was done with standard colony counting method.

obtained from conventional colony counting method. Hence, it can be concluded that the Ab/$Cu_3(BTC)_2$-PANI /ITO biosensor can offer a rapid and accurate option for the selective analysis of *E. coli* in different environmental samples.

4. Conclusions

In the present work, the utility of a new Ab/$Cu_3(BTC)_2$-PANI/ITO biosensor has been demonstrated successfully as an efficient electrochemical biosensing platform for highly sensitive detection of *E. coli*. The proposed sensor offers a quick response time, desired selectivity, and a very low limit of detection. The fabrication process of the biosensor is also simple (e.g., without requiring cumbersome steps). Due to a very large surface area of the developed transduction platform (i.e., $Cu_3(BTC)_2$-PANI composite), it has been possible to operate the sensor for a wide range of analyte concentration at a sufficiently low limit of detection.

In comparison to other electrochemical platforms (e.g., graphene and CNTs), the herein proposed MOF based biosensor is advantageous to offer a better control on final material and surface characteristics through facile fabrication. From an environmental perspective, this MOF based biosensor should be useful with respect to the nanotoxicity concerns, making it more feasible to develop in form of disposable strips. A performance comparison of the Ab/$Cu_3(BTC)_2$-PANI/ITO with the already available electrochemical biosensors of *E. coli* is presented in Table 2 which also suggests that the system proposed in this study should offer an advanced option for the biosensing of *E. coli*.

Acknowledgements

AG thanks the Department of Biotechnology, Ministry of Science and Technology, Government of India for her research fellowship. The financial assistance from a Department of Science and Technology, India (DST, India) project grant (GAP-397) is gratefully acknowledged. Authors are also grateful to the Director, CSIR-CSIO, Chandigarh for providing the necessary research facilities. KHK acknowledges the support made by the R&D Center for Green Patrol Technologies through the R&D for Global Top Environmental Technologies funded by the Ministry of Environment (MOE) as well as by a grant from the National Research Foundation of Korea (NRF) funded by the Ministry of Science, ICT & Future Planning (Grant No: 2016R1E1A1A01940995).

References

Ahmed, I., Jhung, S.H., 2014. Composites of metal–organic frameworks: preparation and application in adsorption. Mater. Today 17, 136–146.
Allendorf, M.D., Stavila, V., 2015. Crystal engineering, structure–function relationships, and the future of metal–organic frameworks. CrystEngComm 17, 229–246.
Ameloot, R., et al., 2009. Patterned growth of metal-organic framework coatings by electrochemical synthesis. Chem. Mater. 21, 2580–2582.
Bhardwaj, N., et al., 2016a. Bacteriophage immobilized graphene electrodes for impedimetric sensing of bacteria (Staphylococcus arlettae). Anal. Biochem. 505, 18–25.
Bhardwaj, N., et al., 2016b. Bacteriophage conjugated IRMOF-3 as a novel opto-sensor for S. arlettae. New J. Chem. 40, 8068–8073.
Bhardwaj, S.K., et al., 2015. Immunosensing of atrazine with antibody-functionalized Cu-MOF conducting thin films. ACS Appl. Mater. Interfaces 7, 26124–26130.
Bhardwaj, S.K., et al., 2017. TCNQ-doped Cu-metal organic framework as a novel conductometric immunosensing platform for the quantification of prostate cancer antigen. Sens. Actuators B: Chem. 240, 10–17.
Buchwalow, I., et al., 2011. Non-specific binding of antibodies in immunohistochemistry: fallacies and facts. Sci. Rep. 1, 28.
Campbell, M.G., Dincă, M., 2017. Metal–organic frameworks as active materials in electronic sensor devices. Sensors 17, 1108.
Chui, S.S.-Y., et al., 1999. A chemically functionalizable nanoporous material [Cu3 (TMA) 2 (H2O) 3] n. Science 283, 1148–1150.
Daoben, Z., et al., 1982. Charge transfer complexes of 3, 3′, 5, 5′-tetra-phenyl-2, 2′-Dithiodipyranylidine (2, 2′ DIPSØ4) with 7, 7′, 8, 8′-Tetracyanoquinodimethane (TCNQ) and iodine. Mol. Cryst. Liq. Cryst. 86, 57–62.
Davydovskaya, P., et al., 2014. Analyte detection with Cu-BTC metal–organic framework thin films by means of mass-sensitive and work-function-based readout. Anal. Chem. 86, 6948–6958.
Deep, A., et al., 2012. Nanostructured polyaniline–silicon substrate for protein biosensing. Sens. Actuators B: Chem. 171, 210–215.
Della Rocca, J., et al., 2011. Nanoscale metal–organic frameworks for biomedical imaging and drug delivery. Acc. Chem. Res. 44, 957–968.
Dos Santos, M.B., et al., 2013. Highly sensitive detection of pathogen Escherichia coli O157: H7 by electrochemical impedance spectroscopy. Biosens. Bioelectron. 45, 174–180.
Guo, H., et al., 2009. "Twin copper source" growth of metal− organic framework membrane: Cu3 (BTC) 2 with high permeability and selectivity for recycling H2. J. Am. Chem. Soc. 131, 1646–1647.
Hassan, A.-R.H.A.-A., et al., 2015. Highly sensitive and rapid determination of Escherichia coli O157: H7 in minced beef and water using electrocatalytic gold nanoparticle tags. Biosens. Bioelectron. 67, 511–515.
Hernandez-Vargas, G., et al., 2018. Electrochemical biosensors: a solution to pollution detection with reference to environmental contaminants. Biosensors 8, 29.
Hosseini, M., et al., 2016. Fabrication of capacitive sensor based on Cu-BTC (MOF-199) nanoporous film for detection of ethanol and methanol vapors. Sens. Actuators B: Chem. 230, 9–16.
Huang, Y., et al., 2011. Graphene-based biosensors for detection of bacteria and their metabolic activities. J. Mater. Chem. 21, 12358–12362.
Israr, F., et al., 2016. Synthesis of porous Cu-BTC with ultrasonic treatment: effects of ultrasonic power and solvent condition. Ultrason. Sonochem. 29, 186–193.
Joung, C.-K., et al., 2013. A nanoporous membrane-based impedimetric immunosensor for label-free detection of pathogenic bacteria in whole milk. Biosens. Bioelectron. 44, 210–215.
Justino, C., et al., 2017. Recent progress in biosensors for environmental monitoring: a review. Sensors 17, 2918.
Kent, C.A., et al., 2011. Light harvesting in microscale metal–organic frameworks by energy migration and interfacial electron transfer quenching. J. Am. Chem. Soc. 133, 12940–12943.
Kokkinos, C., et al., 2015. Quantum dot-based electrochemical DNA biosensor using a screen-printed graphite surface with embedded bismuth precursor. Electrochem. Commun. 60, 47–51.
Kumar, P., et al., 2015. Metal organic frameworks for sensing applications. Trends Anal. Chem. 73, 39–53.
Lei, J., et al., 2014. Design and sensing applications of metal–organic framework composites. Trends Anal. Chem. 58, 71–78.
Li, B., et al., 2014. Porous metal–organic frameworks for gas storage and separation: what, how, and why? J. Phys. Chem. Lett. 5, 3468–3479.
Li, X., et al., 2012. Biocompatibility and toxicity of nanoparticles and nanotubes. J. Nanomater. 2012, 6.
Liu, L., et al., 2018. The applications of metal − organic frameworks in electrochemical sensors. ChemElectroChem 5, 6–19.
Maduraiveeran, G., Jin, W., 2017. Nanomaterials based electrochemical sensor and biosensor platforms for environmental applications. Trends Environ. Anal. Chem. 13, 10–23.
Maes, M., et al., 2010. Separation of C5-hydrocarbons on microporous materials: complementary performance of MOFs and zeolites. J. Am. Chem. Soc. 132, 2284–2292.
Muniesa, M., et al., 2018. Bluephage: a rapid method for the detection of somatic coliphages used as indicators of fecal pollution in water. Water Res. 128, 10–19.
Mustafa, D., et al., 2011. Stability improvement of Cu 3 (BTC) 2 metal–organic frameworks under steaming conditions by encapsulation of a Keggin polyoxometalate. Chem. Commun. 47, 8037–8039.
Peng, L., et al., 2014. Highly mesoporous metal–organic framework assembled in a switchable solvent. Nat. Commun. 5, 4465.
Prestipino, C., et al., 2006. Local structure of framework Cu (II) in HKUST-1 metallorganic framework: spectroscopic characterization upon activation and interaction with adsorbates. Chem. Mater. 18, 1337–1346.
Schlichte, K., et al., 2004. Improved synthesis, thermal stability and catalytic properties of the metal-organic framework compound Cu3 (BTC) 2. Microporous Mesoporous Mater. 73, 81–88.
Schoedel, A., et al., 2016. Structures of metal–organic frameworks with rod secondary building units. Chem. Rev. 116, 12466–12535.
Si, X., et al., 2011. High and selective CO 2 uptake, H 2 storage and methanol sensing on the amine-decorated 12-connected MOF CAU-1. Energy Environ. Sci. 4, 4522–4527.
Thakur, B., et al., 2018. Rapid detection of single E. coli bacteria using a graphene-based field-effect transistor device. Biosens. Bioelectron. 110, 16–22.
Trchová, M., Stejskal, J., 2011. Polyaniline: the infrared spectroscopy of conducting polymer nanotubes (IUPAC Technical Report). Pure Appl. Chem. 83, 1803–1817.
Viswanathan, S., et al., 2012. Electrochemical immunosensor for multiplexed detection of food-borne pathogens using nanocrystal bioconjugates and MWCNT screen-printed electrode. Talanta 94, 315–319.
Wang, Y., et al., 2013. Impedimetric immunosensor based on gold nanoparticles modified graphene paper for label-free detection of Escherichia coli O157: H7. Biosens. Bioelectron. 49, 492–498.
Wang, Y., et al., 2014. Development of a disposable impedance biosensor and its application for determination of Escherichia coli O157: H7. Trans. Asabe 57, 585–591.
Wildeboer, D., et al., 2010. Rapid detection of Escherichia coli in water using a hand-held fluorescence detector. Water Res. 44, 2621–2628.
Wu, Y., et al., 2016. A novel ratiometric fluorescent immunoassay for human α-fetoprotein based on carbon nanodot-doped silica nanoparticles and FITC. Anal. Methods 8, 5398–5406.
Xu, M., et al., 2016. An electrochemical biosensor for rapid detection of E. coli O157: H7 with highly efficient bi-functional glucose oxidase-polydopamine nanocomposites and Prussian blue modified screen-printed interdigitated electrodes. Analyst 141, 5441–5449.
Yan, X., et al., 2014. Extremely enhanced CO_2 uptake by HKUST-1 metal–organic

framework via a simple chemical treatment. Microporous Mesoporous Mater. 183, 69–73.
Zelada-Guillén, G.A., et al., 2010. Real-time potentiometric detection of bacteria in complex samples. Anal. Chem. 82, 9254–9260.
Zeng, T., et al., 2013. A functional rattle-type microsphere with a magnetic-carbon double-layered shell for enhanced extraction of organic targets. Chem. Commun. 49, 6039–6041.
Zhang, Z., et al., 2014. Perspective of microporous metal–organic frameworks for CO 2 capture and separation. Energy Environ. Sci. 7, 2868–2899.
Zhao, D., et al., 2014. Metal–organic frameworks (MOFs) combined with ZnO quantum dots as a fluorescent sensing platform for phosphate. Sens. Actuators B: Chem. 197, 50–57.
Zhu, C., et al., 2014. Electrochemical sensors and biosensors based on nanomaterials and nanostructures. Anal. Chem. 87, 230–249.
Zhu, X., et al., 2013. Metal–organic framework (MOF): a novel sensing platform for biomolecules. Chem. Commun. 49, 1276–1278.